



Evaluation of ice cloud representation in the ECMWF and UK Met Office models using CloudSat and CALIPSO data

Julien Delanoë^{*1,2}, Robin J. Hogan², Richard M. Forbes³, Alejandro Bodas-Salcedo⁴ and Thorwald H. M. Stein²

¹ LATMOS/IPSL/UVSQ/CNRS, Guyancourt, France

² Department of Meteorology, University of Reading, Reading, UK

³ European Centre for Medium-Range Weather Forecasts, Reading, UK

⁴ Met Office, Exeter, UK

*Correspondence to: Julien Delanoë, LATMOS/IPSL/UVSQ/CNRS, 11 Boulevard D'Alembert, 78280 Guyancourt, France. (julien.delanoe@latmos.ipsl.fr)

Ice cloud representation in General Circulation Models (GCMs) remains a challenging task, due to the lack of accurate observations and the complexity of microphysical processes. In this paper, we evaluate the ice water content (IWC) and ice cloud fraction statistical distributions from the Numerical Weather Prediction models of the European Centre for Medium-Range Weather Forecasts (ECMWF) and UK Met Office, exploiting the synergy between the CloudSat radar and CALIPSO lidar. Using the last 3 weeks of July 2006, we analyse the global ice cloud occurrence as a function of temperature and latitude and show that the models capture the main geographical and temperature-dependent distributions, but overestimate the ice cloud occurrence in the Tropics in the temperature range from -60°C to -20°C and in the Antarctic for temperatures warmer than -20°C, but underestimate ice cloud occurrence at very cold temperatures. A global statistical comparison of the occurrence of grid-box mean (IWC) at different temperatures shows that both the mean IWC and the range of IWC increases with increasing temperature. Globally, the models capture most of the IWC variability in the temperature range between -60°C and -5°C. The models also reproduce the observed latitudinal dependencies in the IWC distribution due to different meteorological regimes. Two versions of the ECMWF model are assessed. The recent operational version with a diagnostic representation of precipitating snow and mixed-phase ice-cloud fails to represent the IWC distribution in the -20°C to 0°C range, but a new version with prognostic variables for liquid water, ice and snow is much closer to the observed distribution. The comparison of models and observations provides a much needed analysis of the vertical distribution of ice water content across the globe, highlighting the ability of the models to reproduce much of the observed variability, as well as the deficiencies where further improvements are required.

Copyright © 2011 Royal Meteorological Society

Key Words: model comparison; A-Train; Ice cloud properties

Received ...

Citation: ...

1. Introduction

Despite continuous improvements in ice cloud representation in General Circulation Models (GCMs) in the past decade, these models still need to be improved. It remains a challenging task due to the lack of observations and the complexity of the microphysical processes. These models have large grid-boxes (from 15 km for the latest global ECMWF (European Centre for Medium Range Weather Forecasts) model to 300 km for some climate models), which is incompatible with a detailed description of cloud processes happening at a much smaller scale. We need to understand if, despite their limitations, these models can accurately represent ice cloud properties (Stephens *et al.*

(2002) found more than a factor 2-3 spread in ice water path (IWP) in models), especially the vertical distribution of ice. There are two complementary ways to assess the ability of GCMs to represent cloud properties using active remote sensing observations; comparison of forward modelled measurements using model cloud properties to radar observations (Bodas-Salcedo *et al.* 2008) or lidar observations (Chiriaco *et al.* (2007) and Wilkinson *et al.* (2008)), or direct comparison between retrieved cloud properties from observations with the values in models (e.g. Waliser *et al.* (2009)).

In this present paper, we use the second approach to evaluate the ice water content IWC distribution

in the models of ECMWF and the Met Office. We evaluate two versions of the ECMWF cloud scheme, the operational scheme and a new scheme which is currently being developed. We exploit the synergy of the CloudSat and CALIPSO measurements to retrieve a more accurate IWC and better coverage than a single instrument (Delanoë and Hogan (2008, 2010)). The lidar allows detection of thin ice clouds while radar can penetrate deep ice clouds. For instance, according to Stein *et al.* (2011), the radar and lidar combined estimate of global ice cloud occurrence in the troposphere is 15.1%, whilst the radar and lidar individually only estimate 10.0% and 9.9% of ice cloud occurrence respectively.

The structure of the paper is as follows. In section 2, models, observations and methodology are described. The results of our comparison and our analysis are in section 3 and the conclusion and outlook in section 4.

2. Description of observations, models and methodology

In this section we describe how we derive ice water content using satellite radar-lidar measurements, and how we performed our comparison with ECMWF and UK Met Office model data over the last 3 weeks of July 2006.

2.1. Retrieved ice water content

Ice water content is derived using the variational method of Delanoë and Hogan (2008, 2010), combining CALIPSO (Cloud Aerosol Lidar and Infrared Pathfinder Satellite Observations; Winker *et al.* (2003)) attenuated lidar backscatter and CloudSat (a 94GHz cloud profiling radar, Stephens *et al.* (2002)) radar reflectivity. These two satellites were launched on 28 April 2006. The retrieved IWC is reported at CloudSat's 1 km horizontal resolution and 60 m vertical resolution. We can infer the vertical distribution of detailed ice cloud properties since the radar and lidar backscatter are proportional to very different powers of particle size, so the combination provides accurate particle size with height and hence more accurate IWC than with just one instrument. The Delanoë and Hogan (2010) algorithm retrieves ice cloud properties seamlessly between regions of the cloud detected by both radar and lidar, and regions detected by just one of these two instruments. For instance, when the lidar signal is unavailable (such as due to strong attenuation), the variational framework ensures that the retrieval tends toward similar values to those that would be obtained using an empirical relationship using radar reflectivity factor and temperature (e.g. Liu and Illingworth (2000), Hogan *et al.* (2006), Protat *et al.* (2007)), and when the radar signal is unavailable (such as in optically thin cirrus), accurate retrieval of visible extinction is still possible from the lidar and therefore IWC is retrieved using temperature and extinction. Since the lidar signal is strongly attenuated by liquid water, when supercooled layer is detected, the lidar signal in and below the liquid is not used even if it is identified as also containing ice. In such regions, we assume that radar echo is dominated by the ice, and that liquid attenuation of radar in supercooled clouds can be neglected (Hogan *et al.* 2003), and hence in such a situation, the retrieval reverts back to using reflectivity only. We have also developed a version of the algorithm which assimilates the

infrared radiances (see Delanoë and Hogan (2010)) but it is not used in this paper.

The state vector, which is used to represent retrieved cloud properties, contains visible extinction, extinction-to-backscatter ratio and also a variable related to particle number concentration. At each iteration of the algorithm, the state vector is used to forward model the radar reflectivity and the lidar attenuated backscatter, the latter using the Hogan (2006) multiple scattering model. This process is repeated until convergence. The aim is to find the state vector that minimizes the difference between the observations and the forward model in a least-squares sense. After convergence, the state vector and lookup tables are used to calculate ice water content and effective radius. The forward model assumes a microphysical model describing the shape of the particle size distribution (Delanoë *et al.* 2005) and the relationships between particle mass, cross-sectional area and size. The ice particle mass is assumed to follow the Brown and Francis (1995) mass-size relationship derived from aircraft data. The corresponding area-size relationship is taken from Francis *et al.* (1998), who used the same aircraft dataset as Brown and Francis (1995).

2.2. ECMWF model

In the present paper we compare IWC from the ECMWF IFS (Integrated Forecast System) Cycle 32r3 global model, to IWC derived from the satellite radar-lidar observations. Due to their large grid-boxes, GCMs cannot explicitly represent all the microphysical cloud processes and therefore require parametrizations to represent sub-grid processes. For this study, the horizontal resolution of the model was about 40 km (reduced Gaussian grid) with 91 vertical levels up to 80 km altitude. In the operational model, cloud and large-scale precipitation processes are described by prognostic equations for cloud condensate and cloud fraction, with diagnostic relationships for rain and snow precipitation. The ECMWF cloud scheme is mainly based on the Tiedke (1993) cloud scheme, but has evolved over the past decade. For instance the scheme includes a parametrization of the effects of cloud and precipitation overlap (Jackob and Klein 2000) and an ice supersaturation scheme (Tompkins *et al.* 2007). Grid-box mean specific humidity, grid-box mean cloud condensate and cloud fraction are prognostic variables while liquid and solid precipitation are diagnostic variables. The temperature is used to diagnose the ratio of liquid to ice mixing ratio and allows ice and liquid water to coexist between -23°C and 0°C. The model ice water content used in this analysis is calculated from the grid-box average ice mixing ratio. Every time step a proportion of the ice is converted to a "snow" flux which is then treated diagnostically within the model and removed from the grid column. For comparison purposes, however it is possible to derive the vertical profile of snow water content from the snow flux by assuming a terminal fall velocity for the snow particles (e.g. Hogan *et al.* (2001)). Hereafter this version of the model will be referred to as "ECDiag" model.

As a step towards improving the model, a new scheme has been developed and will be referred to as the ECMWF "ECProg" model in the paper. This new scheme uses separate prognostic variables for cloud liquid water, cloud ice, rain and snow as well as retaining the prognostic cloud fraction of the Tiedke scheme. The liquid water and ice content are therefore now allowed to vary independently

of temperature, removing the need for the diagnostic temperature dependent relationship, and the prognostic representation of snow removes the need to derive the vertical profile from a diagnostic snow flux.

For both schemes ("ECDiag" and "ECProg"), the instantaneous model snapshots are extracted every 3 hours from a series of 12-36 hour forecasts along the CloudSat track to create a continuous time-series of model profiles always within 1.5 hours of the CloudSat overpass time.

2.3. UK Met Office model

The Met Office model used in this study is the MetUM global forecast model at cycle G40, operational from June to September 2006. The horizontal resolution is similar to the ECMWF model, around 40 km at midlatitudes. There are 50 vertical levels up to 63 km. The large-scale cloud scheme is based on Smith (1990), modified to diagnose only the cloud liquid water contents. The model uses the Wilson and Ballard (1999) cloud microphysical scheme for the large scale microphysics, but it has evolved in recent years to incorporate new developments. Water vapour, liquid and ice are now represented as prognostic variables, note that there is no distinction between ice cloud and snow. The convection scheme is based upon Gregory and Rowntree (1990), with cloud base closure for shallow convection based on Grant (2001), and the deep convection CAPE closure of Joseph *et al.* (1980). The convective cloud amount is parameterised as a function of the total convective cloud water, and then expanded into the vertical by a convective anvil scheme Gregory (1999). Water vapour, liquid and ice water contents are defined as mean values in the model grid-box. In contrast to the operational ECMWF model, the ice water content variable includes both "cloud ice" and "precipitating snow". The model data used are similar to that used in Bodas-Salcedo *et al.* (2008); data are produced every 3 h from a two-time step forecast run from each of the four analyses per day at 0, 6, 12 and 18 UTC and from each of subsequent forecast states at T+3. The instantaneous model snapshots are extracted along the CloudSat track to create a continuous time-series of model profiles always within 1.5 hours of the CloudSat overpass time.

2.4. Methodology

As mentioned above, vertical profiles were extracted from both models along the CloudSat-CALIPSO track at the closest time to the observations. IWC retrieved from the A-Train has been averaged to the model grids, using the boundaries of the models boxes. The horizontal resolution of both models is similar, corresponding to around 40 km in midlatitudes and therefore corresponds on average to 40 merged CloudSat-CALIPSO profiles. We only keep boxes filled by at least 20 profiles to avoid representativeness issues, assuming a two dimensional slice is representative of a three dimensional volume (e.g. Illingworth *et al.* (2007)). The CloudSat clutter region which could have contaminated the IWC retrieval when the freezing level reaches the ground has been removed from the statistics for both models and observations.

Two ice water content values are calculated per model grid-box, the all-sky IWC including clear and cloudy parts of the grid-box in the average (hereafter simply IWC), and the in-cloud IWC excluding clear parts ($IWC_{incloud}$,

Table I. Sampling details of the temperature-latitude-IWC frequency calculation

Variable	width	min value	max value
$\log_{10}IWC [kgm^{-3}]$	0.1	-9	-2.5
Temperature [$^{\circ}C$]	4 or 8	-84	4
Latitude [$^{\circ}$]	4	-84	84

hereafter). Both Met Office and ECMWF IWCs are average values in the grid-box, but it is straightforward to calculate in-cloud values using the model cloud fraction. Only observations collected above the freezing level are used in the comparison.

To derive the joint temperature-IWC frequency of occurrence we count the number of data points in each latitude (i_{ϕ}), temperature (i_T), and $\log_{10}(IWC)$ (i_{IWC}) bin for each model and for the observations. This number is denoted $(n(i_T, i_{IWC}, i_{\phi}))$ where i_T , i_{IWC} , and i_{ϕ} are the indices of the temperature, water content and latitude bins respectively. Ranges and bins are summarized in table I for each value. Note that due to the coarser vertical grid resolution in the Met Office model, we need to use a bin size to $8^{\circ}C$ to avoid sampling problems. Once the number of data in each latitude, temperature and $\log_{10}(IWC)$ bin is computed, we need to account for the variation in vertical model levels thickness since they vary with location. For example, the model vertical resolution increases near the ground and therefore a given temperature range will contain more low-level than high-level layers. We also need to take account of the latitude sampling effect, as a larger area is covered in the tropics than near the poles for each latitude bin. A weighting function $W(i_T, i_{IWC}, i_{\phi})$ is derived to account for all these factors and has the following form:

$$W(i_T, i_{IWC}, i_{\phi}) = w(i_T, i_{IWC}, i_{\phi})S(i_{\phi})/N_{\text{profiles}}(i_{\phi}), \quad (1)$$

where $w(i_T, i_{IWC}, i_{\phi})$ represents the sum of the model-layer thicknesses contributing to a bin in km, $S(i_{\phi})$ the surface area at the ground for a $4^{\circ}\text{latitude} \times 4^{\circ}\text{longitude}$ box and $N_{\text{profiles}}(i_{\phi})$ the number of model columns in each latitude bin.

Using the weighting function in (1) we derive the joint temperature-IWC frequency of occurrence by performing a weighted average of the contributions from each latitude:

$$N(i_T, i_{IWC}) = \frac{\sum_{i_{\phi}=1}^n W(i_T, i_{IWC}, i_{\phi})n(i_T, i_{IWC}, i_{\phi})}{\sum_{i_{\phi}=1}^n W(i_T, i_{IWC}, i_{\phi})}. \quad (2)$$

3. Results

3.1. Example of a cross-section of ice water content

Fig. 1 represents an example of an along-track cross section (latitude versus altitude) comparing the grid-box average IWC profiles from the observations to the two ECMWF schemes ("ECDiag" and "ECProg") and the Met Office operational model.

We note, from this example, that both models appear to produce too much ice (in terms of ice presence and not in terms of ice content value) in large cloud systems but do not seem to capture the thin ice cloud above 12 km

between -20° and -5° latitude. Globally, the observations show higher values and higher variability than the models, especially when comparing to “ECDiag” model. Only IWC from the condensed water prognostic variable is represented in the “ECDiag” model (Fig. 1d) whereas the IWC from the “ECProg” model (Fig. 1e) includes both ice and snow prognostic variables. Note that “ECDiag” scheme fails to reproduce the observed increase in IWC near the melting layer region. This occurs for two reasons; firstly because the fraction of cloud condensate that is ice (rather than super-cooled water) is a diagnostic function of temperature decreasing from 100% at -23°C to zero at the melting level, and secondly because the diagnostic snow flux is not included in the comparison (as it is not seen by the radiation scheme in the model). The “ECProg” and Met Office models appear to be more realistic in comparison with the observations, with the maximum IWC in deep precipitating systems just above the melting layer.

3.2. Ice water path comparison

In this section, we compare global vertically integrated ice water path (IWP) over the last 3 weeks of July 2006. Global maps of the IWP distribution for the Met Office and ECMWF (“ECDiag” and “ECProg”) models and observations are presented in Fig. 2. IWP values are averaged in 8° latitude by 10° longitude boxes. Observations on the model grids (top panels) show high values along the inter-tropical convergence zone (ITCZ), in West Africa corresponding to the beginning of the West African monsoon and in southern midlatitudes, but also very small IWP values in North Africa and North Australia. A large cloud-free area is observed along the -20° parallel related to the descending branch of the Hadley cell. It is clearly shown that models capture global patterns but they underestimate global mean IWP. This is especially true for “ECDiag” model, which does not include snow in the ice variable. Note that the mean can be misleading because it is strongly weighted to the very high values, which is why we now look at the normalised probability distribution functions (hereafter pdf) of IWP.

These results are consistent with Fig. 3, which shows the pdf of IWP for the ECMWF and Met Office models, and it can be seen that the distribution peaks are all centred around the same value of $2 \times 10^{-2} \text{ kg m}^{-2}$. Globally, observations on the two model grids are very similar (thick black line for the Met Office and thin black line for ECMWF grid); the main difference between the model grids is the vertical resolution, which has a small impact on IWP due to the integrated nature of this variable. The Met Office and “ECProg” models seem to capture the IWP distribution reasonably well, although both models produce more small values and fewer high values than observed. The “ECDiag” model, which does not include snow in its ice variable, shows a rapid reduction in occurrence above 0.2 kg m^{-2} . However as mentioned earlier, the diagnostic snow flux variable can be used to derive an equivalent snow water content which can be added to the IWC and the dashed grey line is obtained showing a more comparable distribution to the observations. However, this snow is not used in the radiative calculation in the current version of the model. This problem is overcome using the new scheme with radiatively active prognostic ice and snow variables but it still slightly underestimates IWP values.

Note that IWP is mainly dominated by the large IWC values, and therefore radar on its own would already provide a good estimate of mean IWP and the full pdf assuming that the relationship between high reflectivity and IWC is accurate enough. This explains why our results are similar to those found by Waliser *et al.* (2009) in their Fig. 4e for one complete year of CloudSat IWP retrieval. Both IWP distributions, CloudSat and ours, exhibit the same patterns with high values along the ITCZ but also a large cloud free area along the -20° parallel.

3.3. Ice cloud fraction comparison

In this section, we exploit the benefits of combining both radar and lidar measurements to describe the vertical distribution of IWC. As shown previously, the models capture the distribution of the mean IWP reasonably well, but this does not ensure that the mean IWC is correctly represented. Compensatory effects can artificially give good results for IWP, for example, when the models tend to produce more ice clouds with lower IWC values. For radiation, a correct mean IWP is not enough and a good representation of the distribution of IWC is mandatory.

We now examine ice cloud occurrence as a function of temperature, altitude and latitude. Fig. 4 presents the latitude versus temperature and latitude versus height representations of ice cloud occurrence (fraction of the time when mean grid-box IWC is greater than 10^{-6} g m^{-3}) for the observations and the models. It shows that the models capture globally the main structures in ice cloud occurrence, for example there are few ice clouds around latitude of -20° which is expected due to the subsidence associated with

the descending branch of the Hadley cell in the southern (winter) hemisphere. However, both models overestimate ice cloud occurrence in Tropics, by up to 0.2 for ECMWF between -60°C and -20°C . A similar result was found by Wilkinson *et al.* (2008); they used 15 days of the Ice Cloud and Land Elevation Satellite (ICESat) lidar to evaluate ECMWF ice cloud fraction. They showed that the ECMWF model (IFS cycles 26r1 and 26r3) simulated the occurrence and location of cloud well but overestimated the mean amount of ice cloud, particularly in tropics. We also find that the two versions of ECMWF model overestimate ice cloud occurrence in the tropics for very cold temperatures between 10° and 20° latitude.

All models overestimate ice cloud occurrence in the Antarctic for temperatures warmer than -20°C , due to the fact that the models tend to overestimate the ice precipitation in that area and one does not separate cloud from ice precipitation. This is particularly unexpected for the ECMWF current model which does not include snow in its cloud variable. This overestimation could be also explained by the fact that models have difficulty producing supercooled liquid layer in this region and therefore would produce too much ice instead. On the other hand, the observations exhibit more ice clouds in this region at very cold temperatures, between -80°C and -60°C and 9 km and 16 km. This discrepancy originates from the presence of polar stratospheric clouds (PSCs) in this region, which will be discussed in section 3.4.

The cloud phase issue is also evident in Fig. 4, where we can clearly see the impact of the liquid/ice partition in the ECMWF “ECDiag” model. There is an particularly obvious step change in frequency of occurrence at about -23°C in the southern middle latitudes. However this is less

visible in both the ECMWF “ECProg” and the Met Office models.

3.4. Ice water content comparison

A common way to represent the IWC distribution at global scale is the zonal distribution of mean grid-box IWC as a function of height. Fig. 5 shows the zonal distribution for both models and observations. Note that the contours of the distributions are not fully consistent with the ice cloud occurrence distribution (Fig. 4) since very small cloud occurrences are represented in Fig. 5 while cloud fraction below 0.1 is shown in white in Fig. 4. This is a deliberated choice to show the fine structure of IWC distribution. It is interesting to see that models tend globally to overestimate the ice cloud fraction (Fig. 4) but cannot reproduce at each latitude the largest values of IWC derived from the observations and this is particularly true for the ECMWF “ECDiag” model. This statement reinforces the idea that a simple analysis of IWP would not allow us to show the compensating effects already mentioned in the previous section. Once again, models capture globally the main structures in mean grid-box IWC apart from the high clouds above the South Pole. The Met Office model reproduces both structures and IWC values (although large IWC values are slightly underestimated) in the regions from the middle latitudes to the poles but clearly underestimates IWC values in the tropical belt region below 12 km. The ECMWF “ECDiag” model is the one showing the poorest IWC distribution: mean grid-box IWC values are strongly underestimated whatever the latitude and only the structure of IWC with values below 0.001 g m^{-3} are correctly represented. Fortunately, the ECMWF “ECProg” model seems to better represent the zonal distribution and results are similar to the Met Office apart from the tropical belt region where “ECProg” model produces higher content than the Met Office model.

Unfortunately, mean grid-box IWC zonal distribution is rather limited since it cannot represent the IWC variability at a given temperature or height and large values of IWC dominate the distribution. Therefore a statistical comparison of the weighted occurrence of grid-box average IWC at different temperatures is presented in Fig. 6 to illustrate this variability. These graphs have been derived using the methodology described in section 2.4, using a weighting function depending on latitude. Each panel shows the frequency of occurrence as a function of temperature (from -80 to 0°C) for the observations at each model grid, and the corresponding model values for different geographical regions.

As mentioned in the previous section, Fig. 4 suggests the presence of PSCs in the Antarctic region. These clouds have to be treated with caution as they are made of either ice or nitric acid drops where the microphysical assumptions in the retrieval are unlikely to be valid and the latter are not represented in the models and therefore are not included in our comparison. Fig. 7 shows the impact of the presence of PSCs in the Antarctic, the weighted occurrence of grid-box average IWC at different temperature for the observations at each model grid is represented; including all clouds in upper panels and when PSCs are removed in lower panels (i.e we remove all the clouds above 9 km between -84° and -60° latitude corresponding to temperatures colder than -60°C).

Global observations (Fig. 6, top panel), when PSCs are removed, show that IWC increases with temperature

on average, with warmer temperatures being associated with larger water contents but also larger variability. The observations on the ECMWF grid, which has higher vertical resolution than the Met Office model, appear to show a large occurrence of IWC between $5 \times 10^{-4} \text{ g m}^{-3}$ and $5 \times 10^{-3} \text{ g m}^{-3}$ colder than -70°C . Globally, the models can capture most of the observed variability in the temperature region between -60°C and -5°C with the right general trend. However, the ECMWF “ECDiag” model does not perform well in the -20°C to 0°C range due the diagnostic snow parametrization mentioned in the previous sections. For instance, the maximum IWC reaches 0.05 g m^{-3} only rarely, while the observed IWC can reach 1 g m^{-3} . The IWC cut-off can be explained by the parametrization of the ice-to-snow autoconversion rate, which follows the exponential formulation of Sundqvist (1978) with a rate coefficient based on Lin *et al.* (1983) and a critical specific ice water content of 0.03 g kg^{-1} . The rate of conversion of the prognostic cloud ice variable to the diagnostic snow variable increases rapidly once ice water contents are higher than the critical value. The diagnostic mixed-phase assumption also becomes important as temperature approach 0°C by reducing the fraction of the condensate that is allowed to be frozen. In contrast, the ECMWF “ECProg” and Met Office models give better results and produce large IWC although are still smaller than those observed. The Met Office model is the one giving the best results in term of general trend and the large variability observed near the melting layer, and it also shows two peaks with slightly higher occurrence of IWC at 10^{-4} g m^{-3} and $5 \times 10^{-2} \text{ g m}^{-3}$. Even though both the Met Office and ECMWF “ECProg” models work reasonably well within the range -60°C to -5°C , they underestimate the frequency of occurrence of the lower IWC at temperatures below -70°C .

Breaking the statistics down into different regions confirms these conclusions. Fig. 6 clearly shows that the models tend to reproduce the observed latitudinal dependencies due to different meteorological regimes. However, the ECMWF model (both schemes) seems to be inclined to show more variability with latitude. For example, ECMWF “ECProg” model does a good job representing the Northern latitude distribution. Regarding the Antarctic, the Met Office model gives better results although underestimating the low IWC occurrence at cold temperatures. The ECMWF “ECProg” model overestimates the occurrence of IWC between -20°C and 0°C .

The high frequency of occurrence of low IWC observed for very cold temperatures originates from the penetration of deep convection to very high altitudes in the tropics. Fig. 4 suggests the mean ice cloud occurrence in the tropics for these cold temperatures ($< -70^\circ\text{C}$) is reasonably well represented by the models. The apparent discrepancy in the tropics in Fig. 6 is partly due to a wider range of lower ice water contents in the model than in the observations, but also due to the contour method for the figures (percentage of data enclosed) which highlights the pattern of the differences more than the quantitative difference in occurrence. The relatively large overestimation of model ice cloud occurrence between -60°C and -20°C , as shown in Fig. 4, dominates the plots.

The IWC distribution analysis in terms of latitude bands shows that the models reproduce the observed latitudinal dependencies. Implicitly this suggests that models can represent the seasonal cycle, since the midlatitude bands in the Northern and Southern hemispheres are showing respectively summer and winter results. However since Northern and Southern hemispheres are not strictly symmetric (ocean cover dominates in the Southern hemisphere), an extra analysis regarding the seasonal variability is shown in Fig. 8, where weighted joint temperature-IWC frequency of occurrence is represented for the observations and “ECDiag” model for both July 2006 and February 2007. It shows clearly that despite a few differences between July 2006 and February 2007 data, the main characteristics are still observed such as the lack of IWC values at cold temperatures and the “ECDiag” model cut-off. It is not shown here but ice cloud occurrence for the observations and “ECDiag” model for both July 2006 and February 2007 shows that our previous conclusion - the model tends to overestimate ice cloud occurrence - is still valid despite some local differences. Note that, as expected, high clouds above Antarctica observed during the Austral Winter (July 2006) are not present during Austral Summer (February 2007). We note also the symmetry Summer/Winter in July and Winter/Summer with few ice clouds around latitude of -20° in July and 20° in February.

3.5. In-cloud ice water content as function of temperature

In this section, the in-cloud IWC ($IWC_{incloud}$ hereafter), defined as the grid-box mean value divided by the cloud fraction, is examined. Fig. 9 depicts the weighted occurrence of $IWC_{incloud}$ distribution at different temperatures for each model and for the observations, including all latitudes. Note that the PSCs have been removed. It is apparent that compared to mean grid-box IWC we find less variability in the Met Office model. Note the opposite behaviour for ECMWF and Met Office models; the Met Office has a very narrow $IWC_{incloud}$ distribution and indeed this distribution looks to be more constrained to a simple function of temperature. On the other hand, none of the models capture the bimodal distribution at temperature warmer than -10°C seen in the observations. These two peaks at $5 \times 10^{-3} \text{ g m}^{-3}$ and 0.1 g m^{-3} appear only for $IWC_{incloud}$. Once again the ECMWF “ECDiag” model suffers from a cut-off at around 0.05 g m^{-3} for the reasons discussed earlier. Our previous remarks concerning low IWC at very cold temperatures are still valid; as all models underestimate the occurrence of low IWC below -65°C although PSCs are removed.

The grid-box mean IWC is a prognostic variable in the Met Office Model and as suggested by [Bodas-Salcedo et al. \(2008\)](#), the fact that the in-cloud value has less variability indicates that the cloud fraction and grid-box mean IWC are positively correlated. This hypothesis is confirmed in Fig. 10 where we can see that small IWC values are associated with small cloud fraction values for given temperature ranges. Therefore small grid-box mean IWC values when divided by small cloud fraction values at a given temperature tend to narrow the $IWC_{incloud}$ distribution. The ECMWF models show much more variability around the general trend and this is particularly true at very cold temperature. This variability is larger than the measured variability. This result is due to the fact that the cloud fraction and grid-box mean IWC are less correlated than

in the case of the Met Office model as illustrated in Fig. 10. Fig. 10 shows clearly the difference in the grid-box mean IWC-cloud fraction relationships for Met Office and ECMWF models, with an apparent symmetry between the high and low cloud fraction in the ECMWF model relationship and no obvious temperature dependence. The most striking result is when one compares the models grid-box mean IWC-cloud fraction relationships with the relationships derived from the observations, the relationships derived from the observations seem to be a mixture of both models relationships. It is also clearly shown that both ECMWF schemes exhibit a cut off in small grid-box mean IWC due to the fact that all cloud with a specific content, less than $10^{-8} \text{ kg kg}^{-1}$, is evaporated to avoid small cloud condensate which are radiatively unimportant. The second cut off only seen ECMWF “ECDiag” model for high grid-box mean IWC is due to the missing snow and does not appear in the ECMWF “ECProg” model.

4. Conclusions and discussion

As GCMs become increasingly sophisticated, there is as strong a need as ever for evaluation with high quality observations to constrain and validate the parametrizations in the models, especially the evaluation of their vertical profile of cloud properties. In this paper we evaluate the operational UK Met Office model and the ECMWF model with two versions of cloud parametrization, using observations from the active remote sensing instruments onboard the CloudSat and CALIPSO satellites. Spaceborne radar and lidar provide an unprecedented opportunity to describe the vertical distribution of clouds across the globe; the radar can penetrate thick ice clouds but its lack of sensitivity for detecting thin ice cloud is compensated by the lidar. The synergy of the CloudSat and CALIPSO measurements to retrieve a more accurate IWC ([Delanoë and Hogan \(2010\)](#)) has been exploited to evaluate the representation of ice water content and ice cloud fraction in the ECMWF and Met Office models.

A first look at ice water path shows that the models have a good representation of the spatial patterns but underestimate the global mean IWP. The larger snow particles make up a significant proportion of the IWP and therefore the ECMWF “ECDiag” model without the snow field significantly underestimates the global mean IWP. The PDFs of the IWP show all models are consistent with the observations in terms of the peak of the distribution at around $2 \times 10^{-2} \text{ kg m}^{-2}$. The particular lack of high IWP in the ice-only field of the ECMWF “ECDiag” model is evident in the PDF with a cut off at about 0.2 kg m^{-2} . In contrast, the Met Office and “ECProg” models capture the IWP distribution reasonably well, although both models underestimate the occurrence of high IWP values and overestimate the number of low values.

We have also examined ice cloud occurrence as a function of temperature, altitude and latitude. The models capture the main structures in ice cloud occurrence but both models globally overestimate ice cloud occurrence in the Tropics between temperatures of -60°C and -20°C . All models also overestimate ice cloud occurrence in the Antarctica region for temperatures warmer than -20°C and underestimate ice cloud occurrence at very cold temperatures, which is likely to be due to the presence of polar stratospheric clouds.

A statistical comparison of the weighted occurrence of grid-box average IWC at different temperatures shows that mean IWC as well as the variability of IWC generally increases with increasing temperature. Globally, the models capture most of the observed variability in the temperature range between -60°C and -5°C with the right general trend. The ECMWF “ECDiag” model misses the high IWC values in the -20°C to 0°C range due to the diagnostic mixed-phase representation and missing snow field, leading to an IWC cut-off at 0.05g m⁻³. The ECMWF “ECProg” and Met Office models give results closer to the observed distributions with larger IWC values, but still underestimate the occurrence of values greater than 5g m⁻³. Even though both the Met Office and ECMWF “ECProg” models have reasonable agreement within the range -60°C to -5°C, they underestimate the frequency of occurrence of the lower IWC at very cold temperatures. The models also reproduce the observed latitudinal dependence in the distributions.

A global comparison of the in-cloud IWC for the models and observations has been calculated by dividing the grid-mean IWC by the grid-box cloud fraction. This is a relevant quantity as it is the in-cloud IWC that is used for the microphysical processes in the cloud parametrizations. The in-cloud IWC is less variable in the Met Office model than in the observations and the ECMWF models. However, neither model captures the bimodal distribution at temperatures warmer than -10°C seen in the observations. The narrower distribution of the in-cloud IWC characterising the Met Office model is due to the fact that the grid-box mean IWC is a prognostic variable and the cloud fraction and grid-box mean IWC are positively correlated at given temperature. The variability in the IWC_{incloud} of the ECMWF model is explained by the fact that the grid-box mean IWC-cloud fraction does not follow the same relationship as the Met Office model including an interesting symmetry between low and high cloud fraction. As a very interesting result, the observed grid-box mean IWC-cloud fraction relationship seems to be a mixture of both models relationships.

In this paper we perform an unprecedented comparison of ice cloud from two operational NWP models with data derived from a combination of CloudSat radar and CALIPSO lidar observations. Although the statistical analysis was limited to 3 weeks of data, this is sufficient to highlight some of the main positive and negative aspects of the models representation of the three-dimensional IWC field across the globe, at least for the northern-hemisphere summer season. The comparison could be extended to look at other seasons and inter-annual variability with the timeseries of data already collected from CloudSat and CALIPSO (as yet more than 4 years) and with the European Space Agency planned launch of the EarthCARE satellite (ESA 2004), hosting a High Spectral Resolution Lidar, a Doppler cloud radar, a Broad Band Radiometer and a Multi-Spectral Imager. In addition, there are some aspects of the comparison that are not investigated in detail in the present paper and will need to be addressed with future work, including:

1. Assessing the representativeness of the observations.

The satellite track represents only a 2D slice through a 3D model grid-box and there is some uncertainty as to the representativeness of these observations for a model 3D grid-box. A statistical approach could be used to evaluate the variability of the

cloud properties and estimate an error due to non-uniform filling (Stiller 2010). However, in this paper the main discrepancies in the statistical analysis between model and observations are significantly larger than any likely error due to representativity. These issues may become more significant for a more detailed verification of the model when a statistical correction approach could be applied or a wider band of radiometric information from the A-Train could be used to reconstruct a 3D scene to extend the radar-lidar measurements to the rest of the 3D grid-box.

2. *Extending the time period for seasonal and inter-annual variations.* In this study the focus was on three weeks of data from the observations and re-runs of the global model simulations for July 2006, sufficient to identify the main features of the model-observation comparison in terms of global statistics and a break down into latitude bands. However, it is planned to extend this study to different seasons and different years to assess seasonal and inter-annual variations.
3. *Using the results to improve ice cloud parametrization.* The focus of this paper is to use observations to validate the ice cloud parametrizations in GCMs and highlights an example of how an improved parametrization scheme in the ECMWF model gives closer agreement with observations in the -20°C to 0°C temperature range (section 3.4). The results also suggest a number of improvements could be made to the ice cloud parametrization in terms of the vertical profile and variability of IWC at different heights/temperatures. For example, changes to the parametrization of aggregation and the sedimentation of ice will effect the vertical profile of ice. Also, the results of section 3.5 showed that the grid-box mean IWC and the cloud fraction in the Met Office model were strongly correlated and therefore these results and those in Bodas-Salcedo *et al.* (2008) would not support a diagnostic ice cloud fraction that monotonically increases with IWC for a given temperature, as currently parametrized in the Met Office model. There is certainly scope for using these results to continue to improve the ice cloud parametrization schemes leading to improvements in the simulation of cloud for NWP and climate.

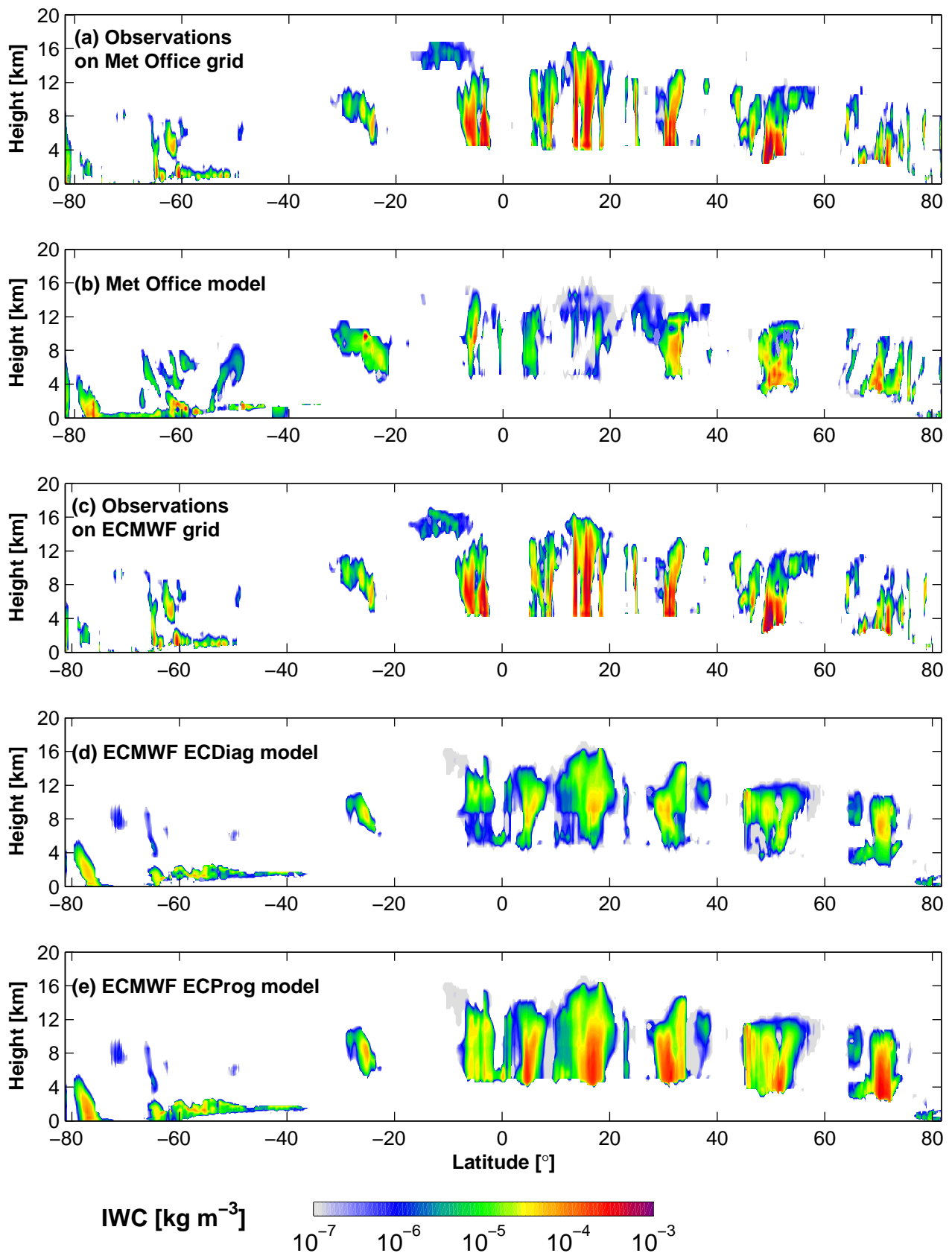


Figure 1. Example of cross-section (latitude vs altitude) of ice water content (kg m^{-3}) for the granule 01118, the 14th of July 2006. Longitude of equator crossing point is 150°. a) All sky grid-box mean IWC derived from CloudSat/CALIPSO measurements using the Delanoë and Hogan (2010) scheme at Met Office resolution. b) Met Office grid-box mean IWC. c) All sky grid-box mean IWC derived from observations on the ECMWF grid. d) ECMWF “ECDiag” model grid-box mean IWC with only one prognostic ice variable. e) ECMWF “ECProg” model averaged grid-box IWC.

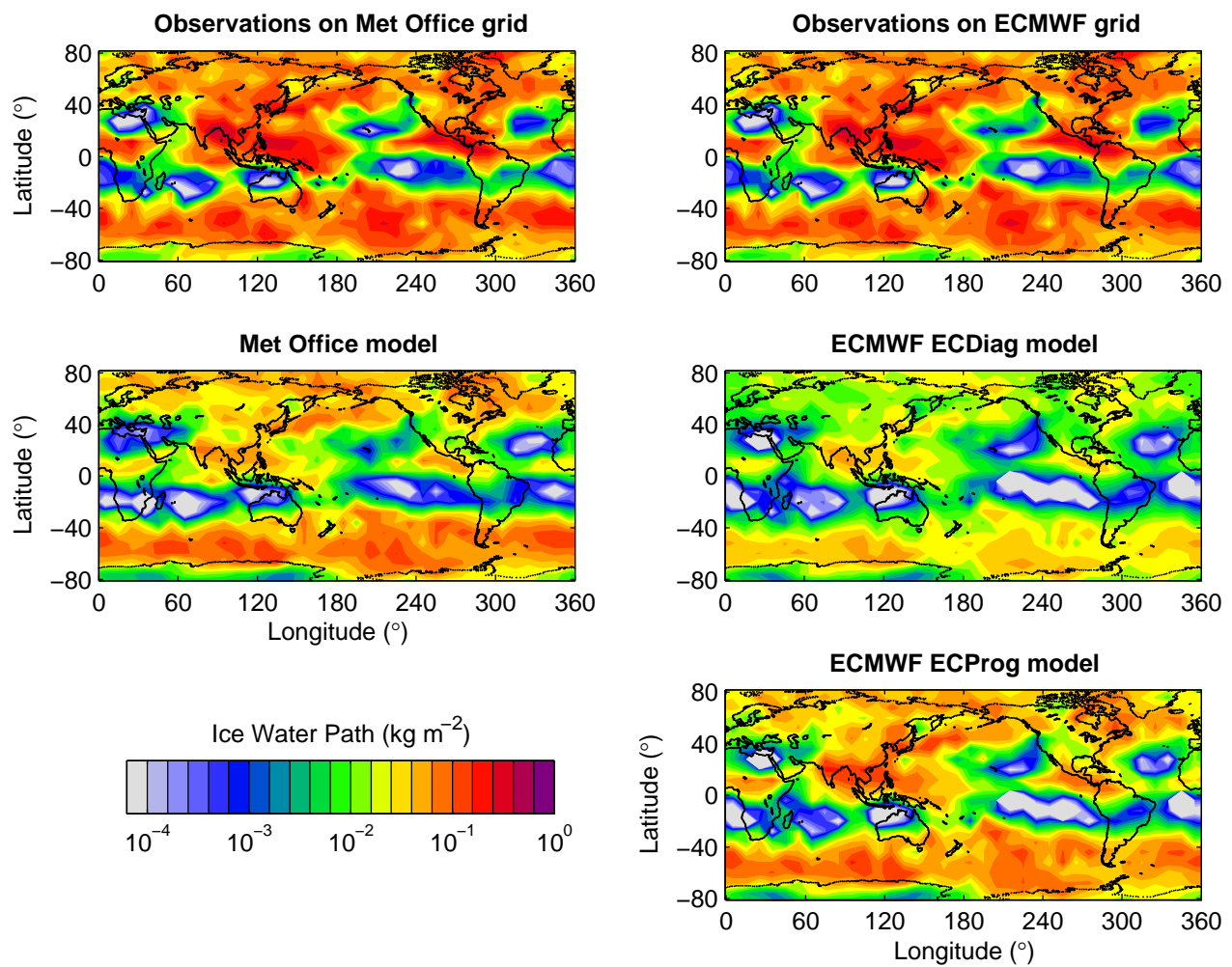


Figure 2. Global maps of all sky mean ice water path for the Met Office and the ECMWF (“ECDiag” and “ECProg”) models and observations during the last three weeks of July 2006. IWP values are averaged in 8° latitude by 10° longitude boxes.

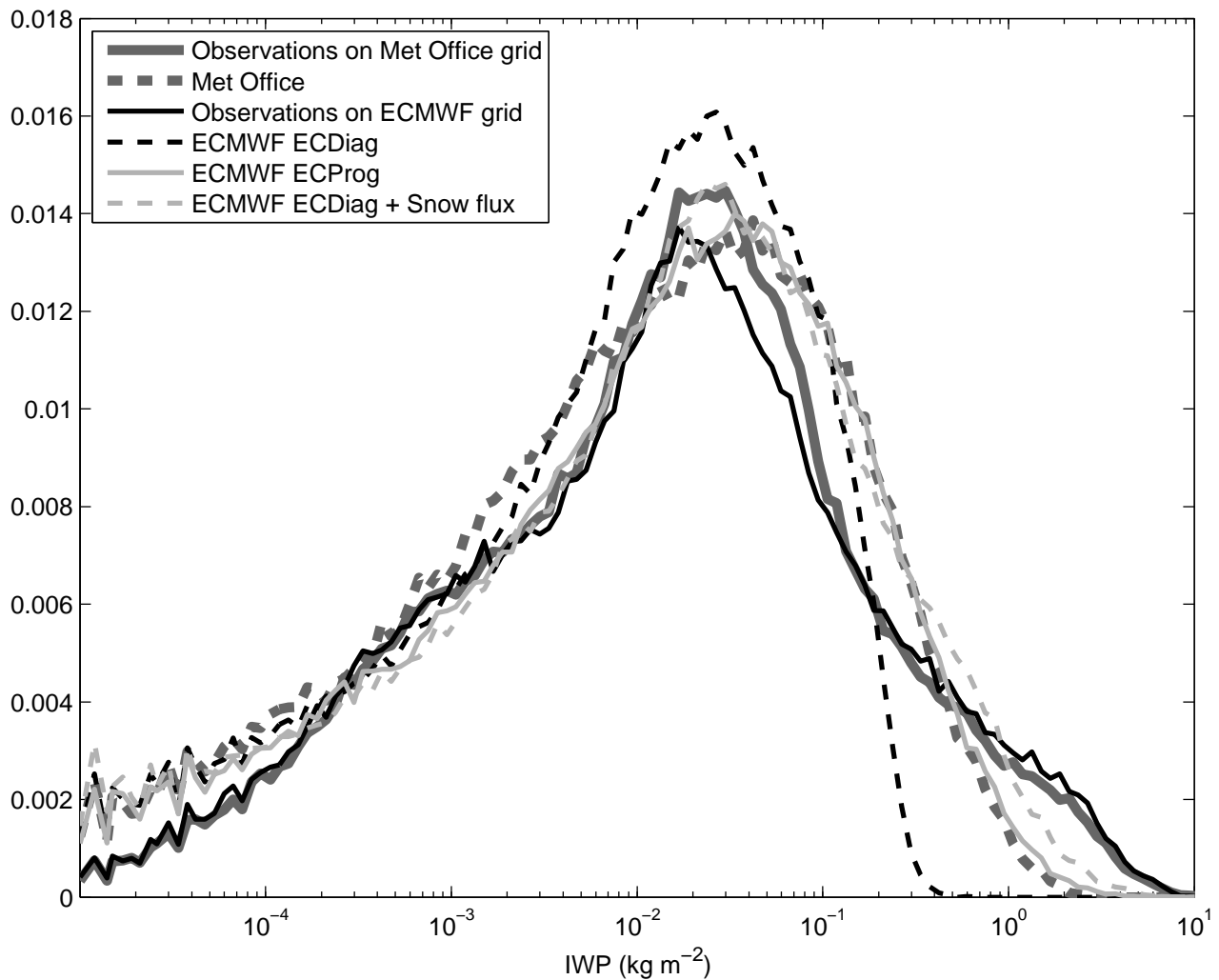


Figure 3. Normalised probability distribution function (pdf), of the ice water path for Met Office and ECMWF models and observations. See text for description.

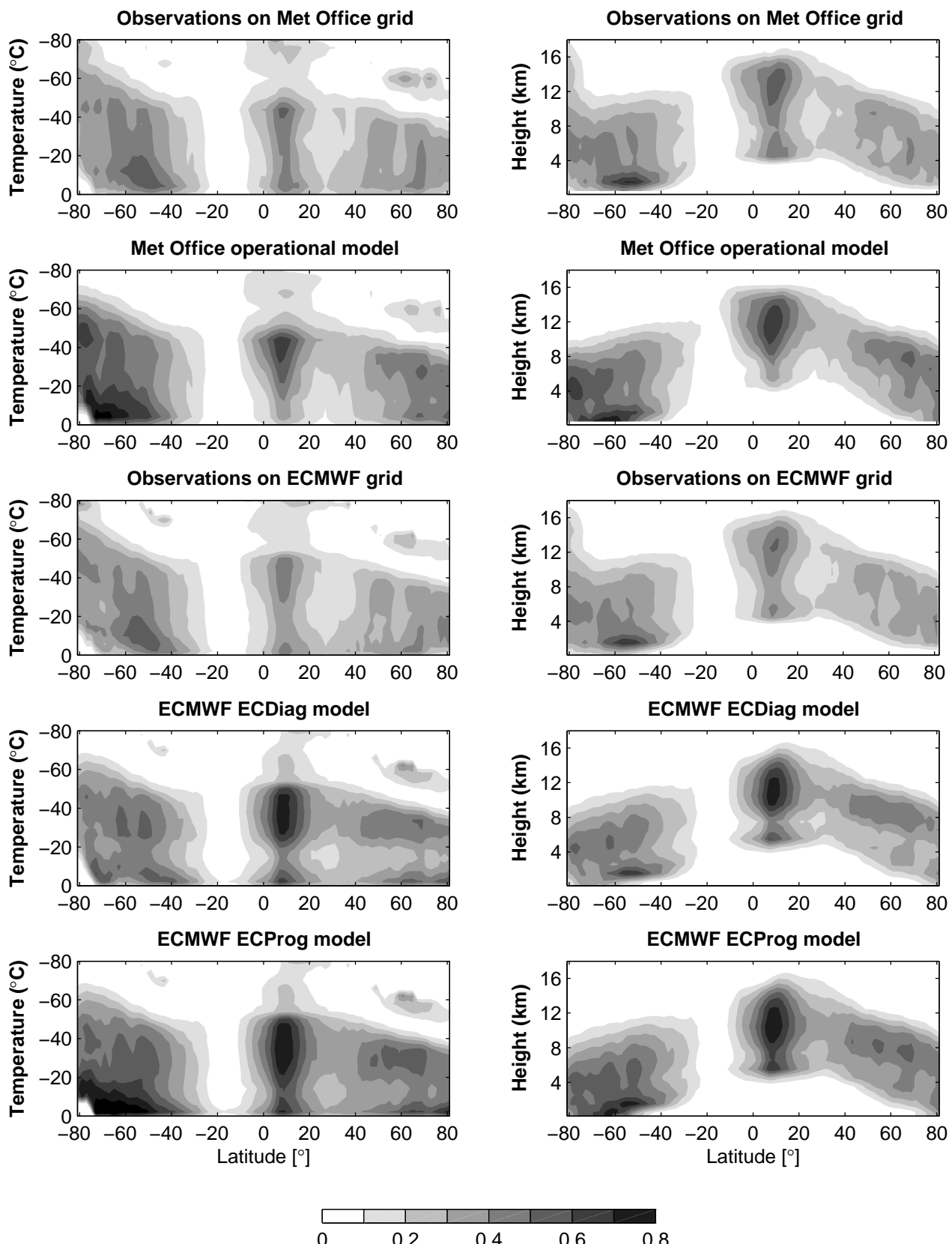


Figure 4. Latitude versus temperature (left column) and latitude versus height (right column) representations of the mean ice cloud occurrence; panels from the top to the bottom: observations on Met Office grid, Met Office values, observations on ECMWF grid, ECMWF “ECDiag” and ECMWF “ECProg” model values.

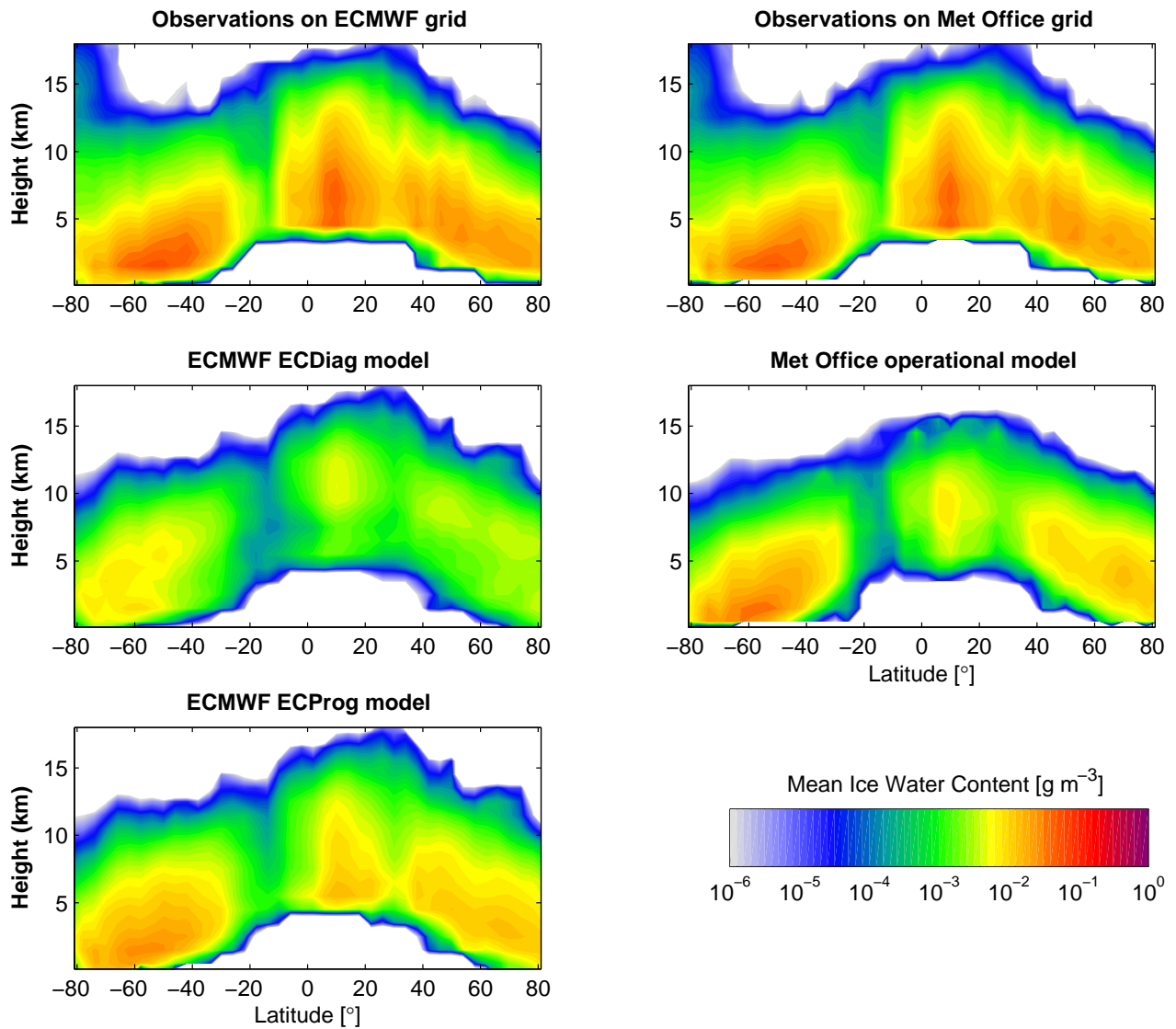


Figure 5. Zonal representation of the mean grid-box IWC; top left panel represents observations on ECMWF grid, middle and bottom left panels are ECMWF “ECDiag” and ECMWF “ECProg” model values. Top and middle right panels illustrate observations and model values on Met Office grid.

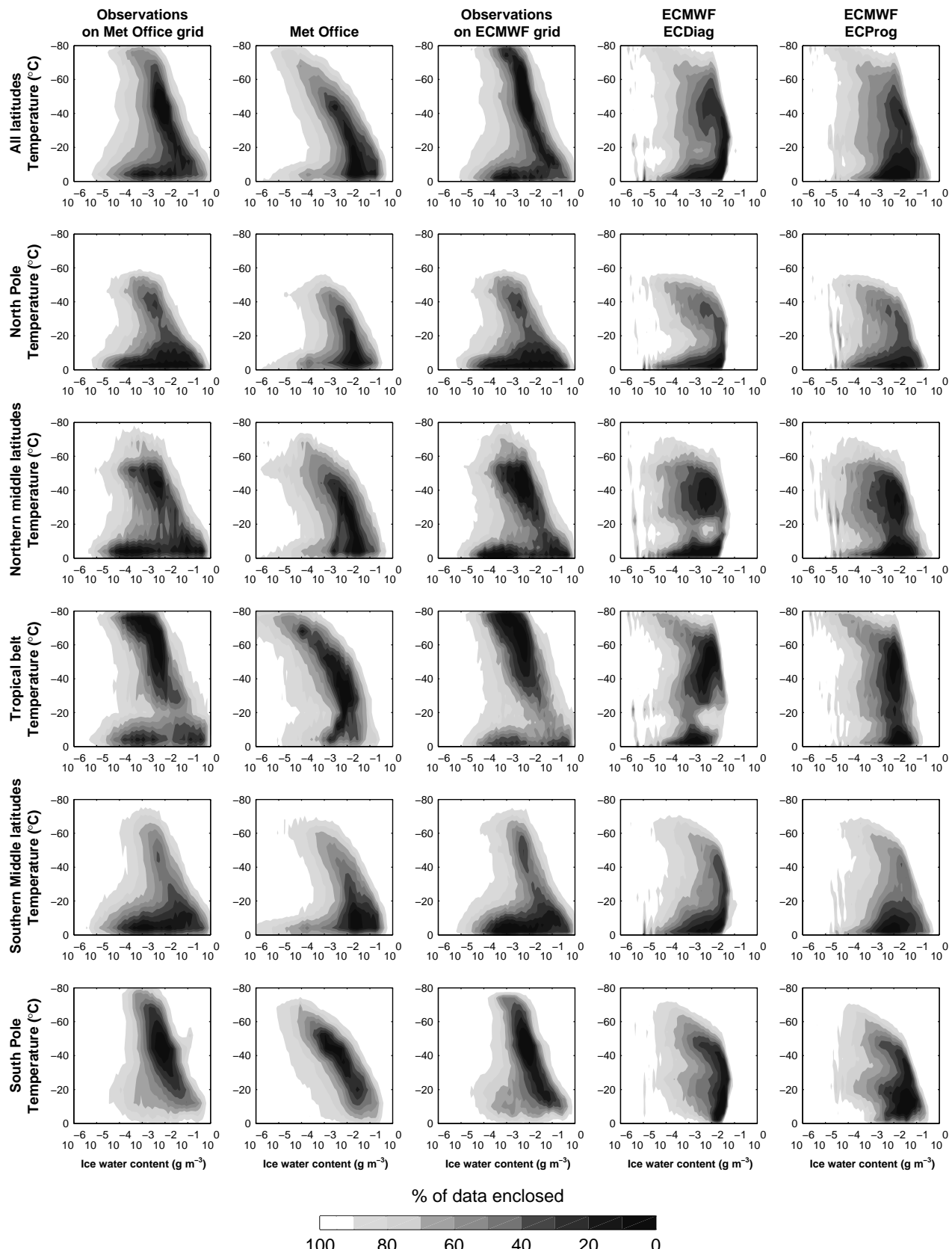


Figure 6. Weighted joint temperature-IWC frequency of occurrence for the observations on Met Office and ECMWF model grids and model values (including Met Office, “ECDiag” ECMWF, “ECProg” ECMWF) for different geographical regions (from the top to the bottom: global, north pole, northern midlatitudes, tropics, southern midlatitudes and south pole). The contours show the percentage of data enclosed within each contour to highlight the spatial patterns in the data.

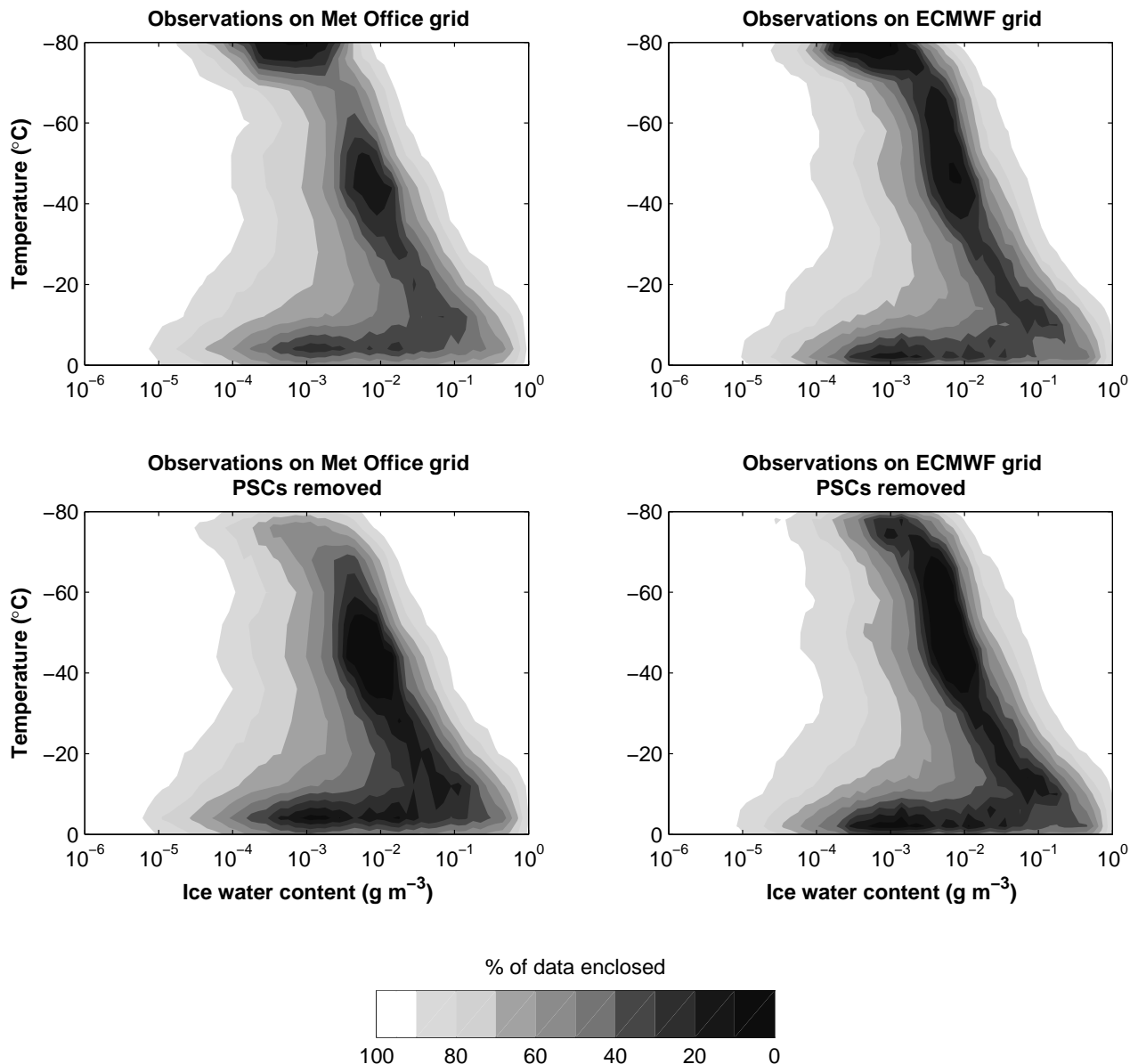


Figure 7. Weighted joint temperature-IWC frequency of occurrence for the observations at each model grid. Bottom panels are identical to the Fig. 6. The contours show the percentage of data enclosed within each contour to highlight the spatial patterns in the data.

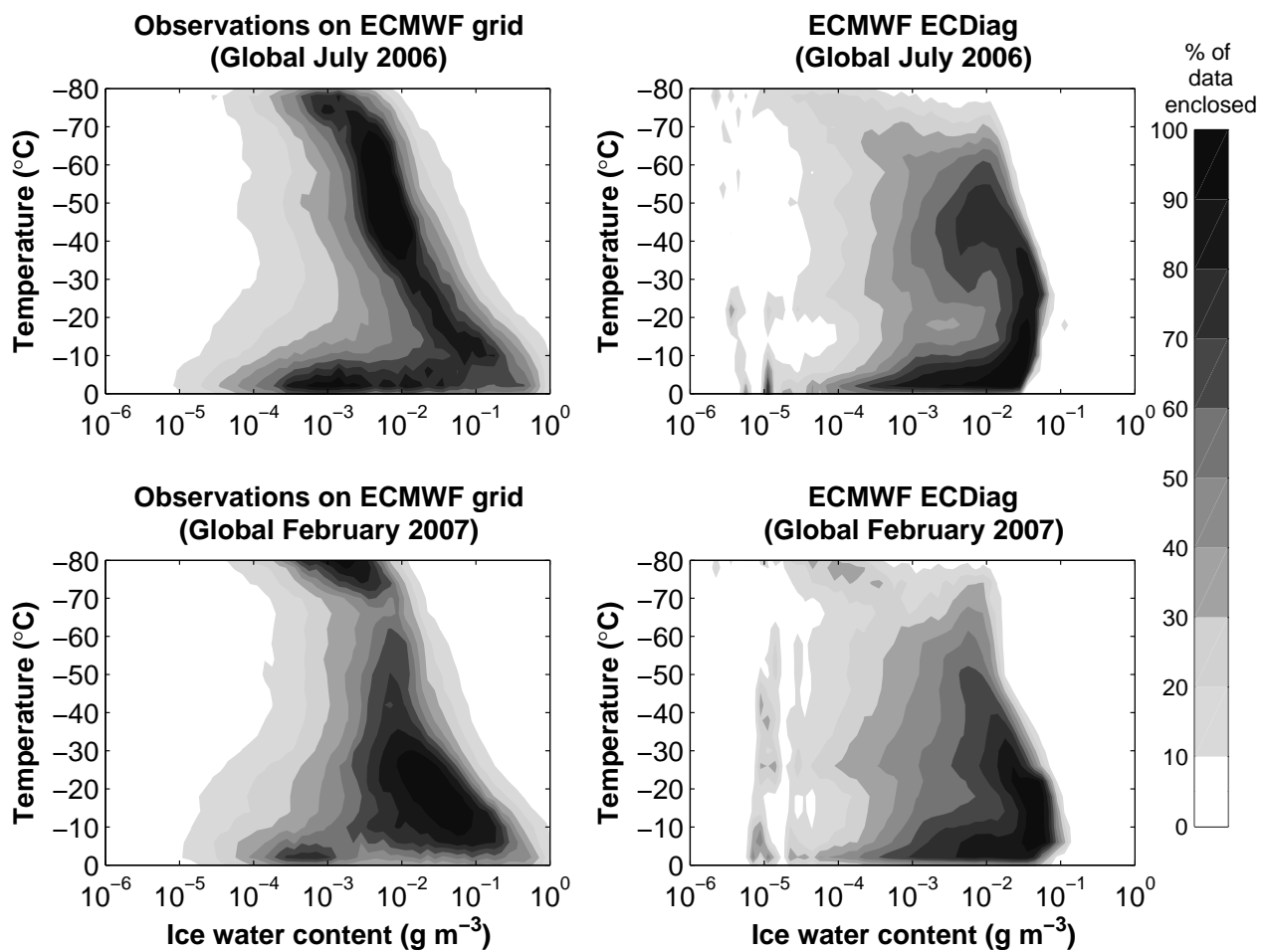


Figure 8. Weighted joint temperature-IWC frequency of occurrence for the observations on ECMWF model grid and “ECDiag” model values for July 2006 and February 2007.

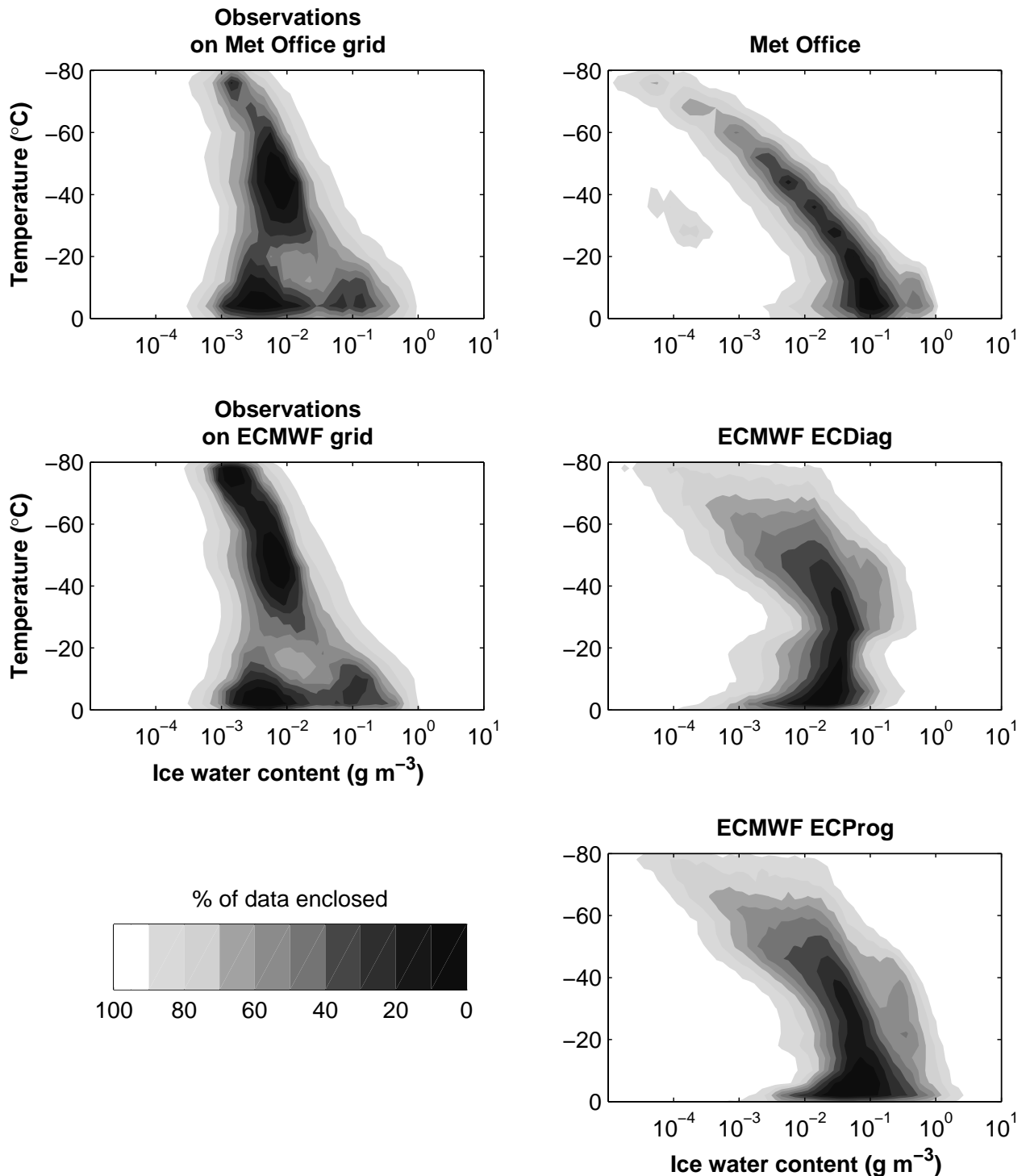


Figure 9. Weighted joint temperature and $\text{IWC}_{\text{incloud}}$ frequency of occurrence for the observations at each model grids in the left column and model values (including Met Office, ECMWF “ECDiag” model, ECMWF “ECProg” model) in the right column . The contours show the percentage of data enclosed within each contour.

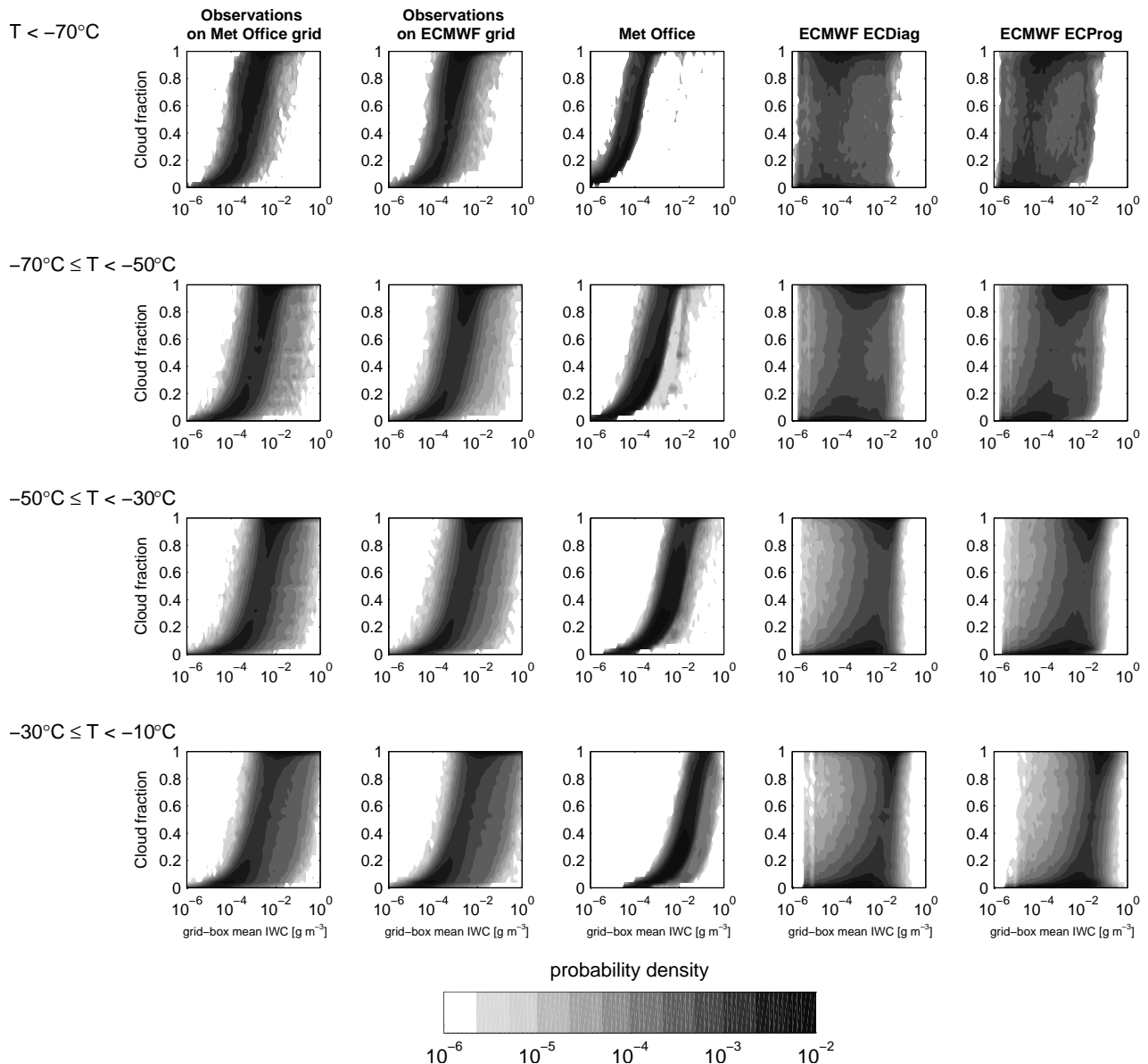


Figure 10. Joint distribution of cloud fraction and grid-box mean IWC for given temperature ranges, for the observations on the Met Office and ECMWF model grids and for the model values (including Met Office, ECMWF “ECDiag” model). The contours show the density of probability.

Acknowledgement

This work was supported by NERC grants NE/C5196971 and NE/H003894/1. Dr. A. Bodas Salcedo was supported by the joint DECC and Defra Integrated Climate Programme, DECC/Defra (GA01101). Data provided by NASA/CNES. We thank the ICARE Data and Services Center for providing access to the data used in this study. We thank the ICARE Data and Services Center for providing data processing.

References

- Bodas-Salcedo A, Webb MJ, Brooks ME, Ringer MA, Williams KD, Milton SF, Wilson DR. 2008. Evaluating cloud systems in the met office global forecast model using simulated cloudsat radar reflectivities. *J. Geophys. Res.* **113**: 1–18, qj.00010.1029/2007JD009620.
- Brown PRA, Francis PN. 1995. Improved measurements of the ice water content in cirrus using a total-water probe. *J. Atmos. Oceanic. Technol.* **12**: 410–414.
- Chiriaco M, Chepfer H, Minnis P, Haefliger M, Platnick S, Baumgardner D, Dubuisson P, McGill M, Noël V, Pelon J, Spangenberg D, Sun-Mack S, Wind G. 2007. Comparison of CALIPSO-Like, LaRC, and MODIS Retrievals of Ice-Cloud Properties over SIRTA in France and Florida during CRYSTAL-FACE. *J. Appl. Meteorol. Climatology* **46**: 249–272, qj.00010.1175/JAM2435.1.
- Delanoë J, Hogan RJ. 2008. A variational scheme for retrieving ice cloud properties from combined radar, lidar and infrared radiometer. *J. Geophys. Res.* **113**: D07204, qj.00010.1029/2007JD009000.
- Delanoë J, Hogan RJ. 2010. Combined CloudSat-CALIPSO-MODIS retrievals of the properties of ice clouds. *J. Geophys. Res.* **115**: D00H29, qj.00010.1029/2009JD012346.
- Delanoë J, Protat A, Testud J, Bouniol D, Heymsfield AJ, Bansemier A, Brown PRA, Forbes RM. 2005. Statistical properties of the normalized ice particle size distribution. *J. Geophys. Res.* **110**: 10201, qj.00010.1029/2004JD005405.
- ESA. 2004. EarthCARE - Earth Clouds, Aerosols and Radiation Explorer European Space Agency SP-1279(1)—The six candidate Earth Explorer Missions ESA/ESTEC, Noordwijk, The Netherlands.
- Francis PN, Hignett P, Macke A. 1998. The retrieval of cirrus cloud properties from aircraft multi-spectral reflectance measurements during EUCREX'93. *Quart. J. Roy Meteorol. Soc.* **124**: 1273–1291.
- Grant A. 2001. Cloud-base fluxes in the cumulus-capped boundary layer. *Quart. J. Roy Meteorol. Soc.* **127**: 407–421.
- Gregory D, Rowntree PR. 1990. A mass flux convection scheme with representation of cloud ensemble characteristics and stability dependent closure. *Mon Weath. Rev.* **118**: 1483–1506.
- Gregory J. 1999. Representation of the radiative effects of convective anvils. *Hadley Centre Technical Note No. 7*. [Http://www.hadleycentre.com/research/hadleycentre/pubs/HCTN/index.html](http://www.hadleycentre.com/research/hadleycentre/pubs/HCTN/index.html).
- Hogan RJ. 2006. Fast approximate calculation of multiply scattered lidar returns. *Appl. Optics* **45**: 5984–5992.
- Hogan RJ, Francis PN, Flentje H, Illingworth AJ, Quante M, Pelon J. 2003. Characteristics of mixed-phase clouds: Part I: Lidar, radar and aircraft observations from CLARE'98. *Quart. J. Roy Meteorol. Soc.* **129**: 2089–2116.
- Hogan RJ, Jakob C, Illingworth AJ. 2001. Comparison of ecmwf winter-season cloud fraction with radar derived values. *J. Appl. Meteorol.* **40**(3): 513–525.
- Hogan RJ, Mittermaier MP, Illingworth AJ. 2006. The retrieval of ice water content from radar reflectivity factor and temperature and its use in the evaluation of a mesoscale model. *J. Appl. Meteorol. Climatology* **45**: 301–317.
- Illingworth AJ, Hogan RJ, O'Connor EJ, Bouniol D, Brooks ME, Delanoë J, Donovan DP, Eastment JD, Gaussiat N, Goddard JWF, Haefliger M, Klein Baltink H, Krasnov OA, Pelon J, Piriou JM, Protat A, Russchenberg HWJ, Seifert A, Tompkins AM, van Zadelhoff GJ, Vinit F, Willén U, Wilson DR, Wrench CL. 2007. Cloudnet – continuous evaluation of cloud profiles in seven operational models using ground-based observations. *Bull. Am. Meteorol. Soc.* **88**: 883–898, qj.00010.1175/BAMS-88-6-883.
- Jackob C, Klein SA. 2000. A parametrization of cloud and precipitation overlap effects for use in General Circulation Models. *Quart. J. Roy Meteorol. Soc.* **126**: 2525–2544.
- Joseph JH, Wiscombe WJ, Weinman JA. 1980. Numerical prediction of convectively driven mesoscale pressure systems. part i. convective parameterization. *J. Atmos. Sci.* **37**: 1722–1733.
- Lin YL, Farley RD, Orville HD. 1983. Bulk parametrization of the snow field in a cloud model. *J. Climate Appl. Meteor.* **22**: 1065–1092.
- Liu CL, Illingworth AJ. 2000. Towards more accurate retrievals of ice water content from radar measurement of clouds. *J. Appl. Meteorol.* **39**: 1130–1146.
- Protat A, Delanoë J, Bouniol D, Heymsfield AJ, Bansemier A, Brown PRA. 2007. Evaluation of ice water content retrievals from cloud radar reflectivity and temperature using a large airborne in-situ microphysical database. *J. Appl. Meteorol. Climatology* **46**: 557–572.
- Smith RNB. 1990. A scheme for predicting layer clouds and their water content in a general circulation model. *Quart. J. Roy Meteorol. Soc.* **116**: 435–460.
- Stein THM, Delanoë J, Hogan RJ. 2010. A comparison between four different retrieval methods for ice cloud properties using data from CloudSat, CALIPSO, and MODIS. *J. Appl. Meteorol. Climatology*. In press.
- Stephens GL, Vane DG, Boain RJ, Mace GG, Sassen K, Wang Z, Illingworth AJ, O'Connor EJ, Rossow WB, Durden SL, Miller SD, Austin RT, Benedetti A, Mitrescu C, the CloudSat Science Team. 2002. The Cloudsat Mission and the A-Train. *Bull. Am. Meteorol. Soc.* **83**: 1771–1790.
- Stiller O. 2010. A flow dependent estimate for the sampling error. *J. Geophys. Res.* **115**, qj.00010.1029/2010JD013934.
- Sundqvist H. 1978. A parametrization scheme for non-convective condensation including prediction of cloud water content. *Quart. J. Roy Meteorol. Soc.* **104**: 677–690.
- Tiedke M. 1993. Representation of clouds in large-scale models. *Mon Weath. Rev.* **121**: 3040–3061.
- Tompkins AM, Gierens K, Rädel G. 2007. Ice supersaturation in the ECMWF integrated forecast system. *Quart. J. Roy Meteorol. Soc.* **133**: 53–63.
- Waliser DE, Li JF, Woods CP, Austin RT, Bacmeister J, Chern J, Genio AD, Jiang JH, Kuang Z, Meng H, Minnis P, Platnick S, Rossow WB, Stephens GL, Sun-Mack S, Tao W, Tompkins AM, Vane DG, Walker C, Wu D. 2009. Cloud ice: A climate model challenge with signs and expectations of progress. *J. Geophys. Res.* **114**, qj.00010.1029/2008JD010015.
- Wilkinson J, Hogan RJ, Illingworth AJ, Benedetti A. 2008. Use of a lidar forward model for global comparisons of cloud fraction between the icesat lidar and the ecmwf model. *Mon Weath. Rev.* **136**: 3742–3759.
- Wilson DR, Ballard SP. 1999. A microphysically based precipitation scheme for the UK Meteorological Office Unified Model. *Quart. J. Roy Meteorol. Soc.* **125**: 1607–1636.
- Winker DM, Pelon J, McCormick MP. 2003. The CALIPSO mission: Spaceborne lidar for observation of aerosols and clouds. *Proc. SPIE* **4893**: 1–11.